JACS
JOURNAL OF THE AMERICAN CHEMICAL SOCIETY
pubs.acs.org/JACS
Article

Ambient-Temperature Hydrogen Storage via Vanadium(II)-Dihydrogen Complexation in a Metal–Organic Framework

David E. Jaramillo, Henry Z. H. Jiang, Hayden A. Evans, Romit Chakraborty, Hiroyasu Furukawa, Craig M. Brown, Martin Head-Gordon, and Jeffrey R. Long*

Cite This: J. Am. Chem. Soc. 2021, 143, 6248–6256
Read Online
ACCESS | Metrics & More | Article Recommendations | Supporting Information

ABSTRACT: The widespread implementation of H_2 as a fuel is currently hindered by the high pressures or cryogenic temperatures required to achieve reasonable storage densities. In contrast, the realization of materials that strongly and reversibly adsorb hydrogen at ambient temperatures and moderate pressures could transform the transportation sector and expand adoption of fuel cells in other applications. To date, however, no adsorbent has been identified that exhibits a binding enthalpy within the optimal range of −15 to −25 kJ/mol for ambient-temperature hydrogen storage. Here, we report the hydrogen adsorption properties of the metal–organic framework (MOF) $V_2Cl_{2.8}$(btdd) (H_2btdd, bis(1*H*-1,2,3-triazolo[4,5-*b*],[4′,5′-*i*])dibenzo[1,4]dioxin), which features exposed vanadium(II) sites capable of backbonding with weak π acids. Significantly, gas adsorption data reveal that this material binds H_2 with an enthalpy of −21 kJ/mol. This binding energy enables usable hydrogen capacities that exceed that of compressed storage under the same operating conditions. The Kubas-type vanadium(II)–dihydrogen complexation is characterized by a combination of techniques. From powder neutron diffraction data, a V–D_2(centroid) distance of 1.966(8) Å is obtained, the shortest yet reported for a MOF. Using *in situ* infrared spectroscopy, the H–H stretch was identified, and it displays a red shift of 242 cm^{-1}. Electronic structure calculations show that a main contribution to bonding stems from the interaction between the vanadium d_π and H_2 σ^* orbital. Ultimately, the pursuit of MOFs containing high densities of weakly π-basic metal sites may enable storage capacities under ambient conditions that far surpass those accessible with compressed gas storage.

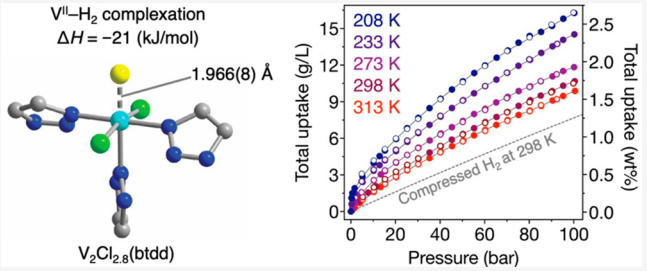

INTRODUCTION

The chemical bond represents one of the smallest units of stored energy.[1] Society has taken advantage of this fundamental unit for decades, to generate power and fuel the transportation sector, by breaking C–H bonds in the combustion of fossil fuels. However, CO_2 emissions from these sectors are among the leading contributors to anthropogenic climate change,[2,3] necessitating a transition to carbon-zero energy systems. With a gravimetric energy density nearly three times that of gasoline and water as its sole product, dihydrogen is poised to play a key role in the transition to a zero-emission energy economy.[4] Indeed, hydrogen is a flexible fuel that can promote renewable energy usage and help transform difficult-to-decarbonize sectors, such as shipping and heavy-duty trucking.[4,5] The hydrogen vision for transportation[6,7] is already being partially realized, as hydrogen fuel-cell light-duty vehicles, trucks, and buses are operating on the road today,[8] with over 40 hydrogen stations in California and over 80 in Germany. While this progress is encouraging, the use of H_2 as a transportation fuel remains a nascent market, and greater adoption and eventual replacement of diesel-powered vehicles are limited in part by the difficulties of on-board hydrogen storage. In particular, limited vehicle space necessitates the use of systems with high volumetric energy densities that can support reasonable driving ranges.[9] Today, on-board hydrogen is stored as a liquid at cryogenic temperatures or, more commonly, as a compressed gas at pressures as high as 700 bar, resulting in hydrogen densities of 70 and 39 g/L, respectively.[10] Both strategies make for costly refueling and require storage systems that can operate reliably under these extreme conditions, but the development of such systems has proven to be difficult.[11] Furthermore, storage of H_2 at 700 bar comes with a significant energy penalty for compression,[12] while also requiring the use of bulky on-board tanks that reduce the overall system volumetric density.[13]

Adsorbent-based systems offer an appealing alternative for high-density hydrogen storage under more mild conditions than cryogenic or highly compressed H_2 storage.[14] While high storage capacities have been achieved using adsorbents at

Received: February 17, 2021
Published: April 14, 2021

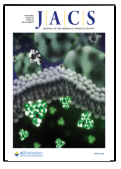

Downloaded via NATL INST OF STANDARDS & TECHNOLOGY on August 2, 2021 at 16:22:42 (UTC).
See https://pubs.acs.org/sharingguidelines for options on how to legitimately share published articles.

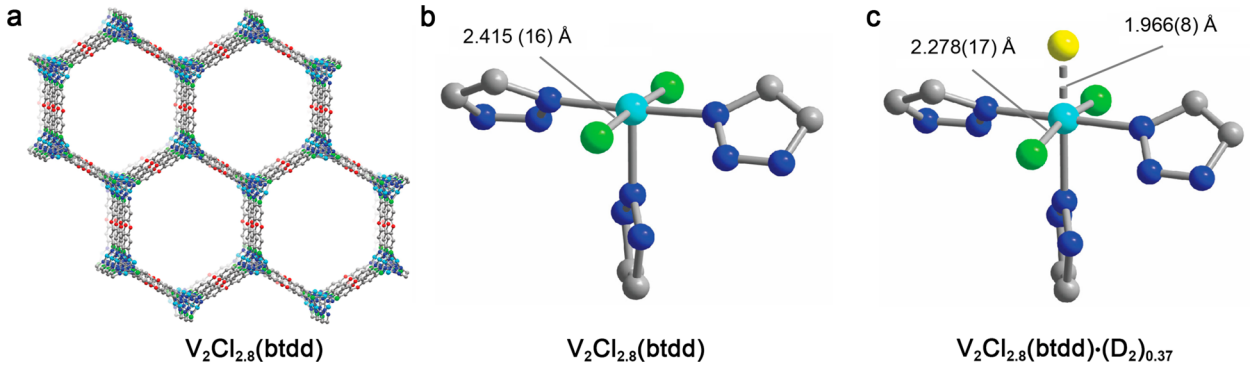

Figure 1. (a) A portion of the structure of $V_2Cl_{2.8}$(btdd) determined from powder X-ray diffraction[44] showing the one-dimensional hexagonal pores. In this material, 60% of the metal sites are coordinatively unsaturated vanadium(II) and 40% are coordinatively saturated vanadium(III). Apical chlorides and hydrogen atoms have been omitted for clarity. (b,c) Structures of the primary vanadium(II) coordination sphere in activated $V_2Cl_{2.8}$(btdd) and $V_2Cl_{2.8}$(btdd) dosed with 0.75 equiv of D_2, determined in this work from Rietveld refinement of powder neutron diffraction data collected at 100 K. Cyan, green, blue, red and gray spheres represent V, Cl, N, O and C, atoms, respectively, while the yellow sphere represents the centroid of an adsorbed D_2 molecule.

cryogenic temperatures,[15−18] this approach is limited in practice due to the need for a cryo-adsorption unit, which significantly reduces the system volumetric density and increases thermal management operating costs.[19−21] Instead, materials capable of ambient temperature on-board H_2 storage have the potential to substantially decrease refueling and infrastructure costs while meeting range requirements. Furthermore, by operating at low pressures (e.g., below 100 bar), lighter, less expensive, and more conformable tanks can be employed.[22] This prospect prompted the US Department of Energy (U.S. DOE), alongside key stakeholders, to define system-level storage performance targets for adsorptive hydrogen storage,[23] including an operating temperature range between −40 and 85 °C and a minimum delivery pressure of 5 bar. Under these or similar conditions, reaching capacities beyond what is possible with compressed H_2 may enable wider use of fuel cells in transportation, as well as other applications, such as stationary backup power.[24]

Maximizing deliverable H_2 capacity under ambient conditions requires that the enthalpy of adsorption fall within the optimal range of −15 to −25 kJ/mol.[23,25,26] However, most materials exhibit enthalpies well outside of this range, resulting in low hydrogen densities (in the case of weak physisorption) or prohibitively high regeneration energies (strong chemisorption).[27] In recent years, crystalline porous metal−organic frameworks (MOFs) have emerged as promising adsorbents for H_2 storage.[28−34] In particular, the vast structural and chemical versatility of these materials makes it possible to tune surface chemistries to increase hydrogen uptake.[16,17] However, most MOFs bind H_2 via weak physisorption with enthalpies near −5 kJ/mol, and therefore maximizing surface area alone is insufficient to achieve a high ambient-temperature uptake. Here, the role of the synthetic chemist is paramount, and, in particular, the installation of coordinatively unsaturated metal nodes can enhance H_2 binding.[32−35] The vast majority of MOFs feature weak-field ligands and high-spin, Lewis-acidic metal sites,[36,37] and strategies to increase H_2 binding enthalpies have thus centered around maximizing metal Lewis acidity. This strategy recently led to Ni_2(*m*-dobdc) (*m*-dobdc^{4-} = 4,6-dioxido-1,3-benzenedicarboxylate), which features a high-density of exposed nickel(II) cations in a square-pyramidal geometry.[38] Strong polarization of H_2 at these sites is augmented by charge transfer from H_2 and gives rise to a binding enthalpy of −12.3 kJ/mol. As a result, Ni_2(*m*-dobdc) is the current benchmark H_2 adsorbent, capable of storing 11.9 g/L of crystal at 298 K and 100 bar.[39]

Despite this progress, substantial improvements are needed to obtain H_2 binding strengths and storage capacities beyond what is possible with 350 or 700 bar compression, motivating the pursuit of alternative approaches for attaining strong metal−H_2 binding in MOFs. Molecular metal−hydrogen chemistry is rich with inspiration for this purpose. Since the discovery of $W(CO)_3(P^iPr_3)_2(\eta^2\text{-}H_2)$ by Kubas and coworkers,[40] complexes containing metal−H_2 modalities abound, featuring π-basic metal sites and dominant orbital interactions.[41] The highest occupied molecular orbital (HOMO) of H_2 is a poor donor,[42] and bonding in Kubas-type complexes is instead dominated by donation of electron density from π-basic metal sites into the σ^* or lowest-unoccupied molecular orbital (LUMO) of H_2. In $W(CO)_3(P^iPr_3)_2(\eta^2\text{-}H_2)$, this orbital interaction gives rise to a binding enthalpy of approximately −80 kJ/mol.[43] Thus, in principle, a less reducing, weaker π-basic metal site should enable realization of H_2 binding enthalpies within the desired range for ambient H_2 storage. In particular, a divalent first-row metal may fulfill these criteria.

We recently reported the first framework containing a high-density of exposed square-pyramidal vanadium(II) sites, $V_2Cl_{2.8}$(btdd) (H_2btdd, bis(1*H*-1,2,3-triazolo[4,5-*b*],[4′,5′-*i*])-dibenzo[1,4]dioxin) (Figure 1a), and demonstrated that the electronic structure of these ions gives rise to orbital-mediated binding and enables highly selective backbonding-based N_2 separations.[44] The empty d_{z^2} orbital in this material is also poised to accept σ donation from the H_2 HOMO, while the partially filled vanadium(II) d_π orbitals provide a pathway for backbonding.[45] Herein, we investigate the H_2 adsorption properties of $V_2Cl_{2.8}$(btdd) and show that it binds H_2 strongly at ambient temperature and pressures, with an H_2 adsorption enthalpy within the optimal range for ambient storage. Significantly, usable hydrogen capacities achieved with this material are greater than those of compressed H_2 under a range of conditions, including 350 bar and 298 K. Powder neutron diffraction enables the first structural characterization of the V^{II}−H_2 interaction (Figure 1b,c), which is further probed through variable temperature *in situ* infrared spectroscopy and computations.

https://doi.org/10.1021/jacs.1c01883
J. Am. Chem. Soc. 2021, 143, 6248−6256

RESULTS AND DISCUSSION

The metal−organic framework $V_2Cl_{2.8}$(btdd) was synthesized as previously reported.[44] Its structure consists of one-dimensional, hexagonal channels with vertices decorated by vanadium sites (Figure 1a). The pore diameter and volume are approximately 22 Å and 1.12 cm^3/g, respectively. This gives rise to a high porosity, and the material exhibits a Langmuir surface area of 3350 m^2/g and a Brunauer-Emmet-Teller (BET) surface area of 1920 m^2/g (Figure S1 and Table S1). The material is mixed-valent, containing 40% vanadium(III) sites, charge-balanced by terminal chloride ligands, and 60% vanadium(II) sites in a square pyramidal geometry.

Low-Pressure H_2 Adsorption. The hydrogen adsorption properties of $V_2Cl_{2.8}$(btdd) were first investigated by measuring low-pressure isotherms up to 1.2 bar. At 77 and 87 K, the isotherms were too steep for meaningful data analysis, and therefore, isotherms were collected near room temperature. Generally, low-pressure H_2 isotherms are not reported at ambient temperatures, given that the typically weak binding operative in physorptive materials makes it difficult to quantify uptake. However, substantial uptake of H_2 occurs in $V_2Cl_{2.8}$(btdd) at 298 K, and the material achieves a capacity of 0.26 mmol/g at 1.2 bar, corresponding to occupation of 10% of the vanadium(II) sites (Figure 2). For comparison, Ni_2(*m*-dobdc) adsorbs just 0.05 mmol/g under the same conditions. At 286 and 273 K, H_2 uptake in $V_2Cl_{2.8}$(btdd) at 1.2 bar increases to 0.36 and 0.49 mmol/g, respectively. A trisite Langmuir−Freundlich equation was used to simultaneously fit the data at three temperatures (Figure 2b, Table S2), and the corresponding fit parameters were used with the Clausius−Clapeyron relation to extract an isosteric heat of adsorption of −20.9 ± 0.2 kJ/mol and an entropy of adsorption of 69.9 ± 0.6 J/(mol·K). Notably, the hydrogen adsorption enthalpy in $V_2Cl_{2.8}$(btdd) is 8.6 kJ/mol greater in magnitude than that determined for Ni_2(*m*-dobdc) but lower than that of Cu-MFU-4*l* (−32.3 kJ/mol), which contains exposed trigonal pyramidal copper(I) sites and exhibits the highest H_2 binding enthalpy of any MOF studied to date.[46] Most importantly, $V_2Cl_{2.8}$(btdd) is the first framework to exhibit a H_2 adsorption enthalpy within the optimal range for ambient-temperature storage, validating the strategy of targeting metal sites capable of orbital-mediated interactions rather than strong Lewis acidic interactions.

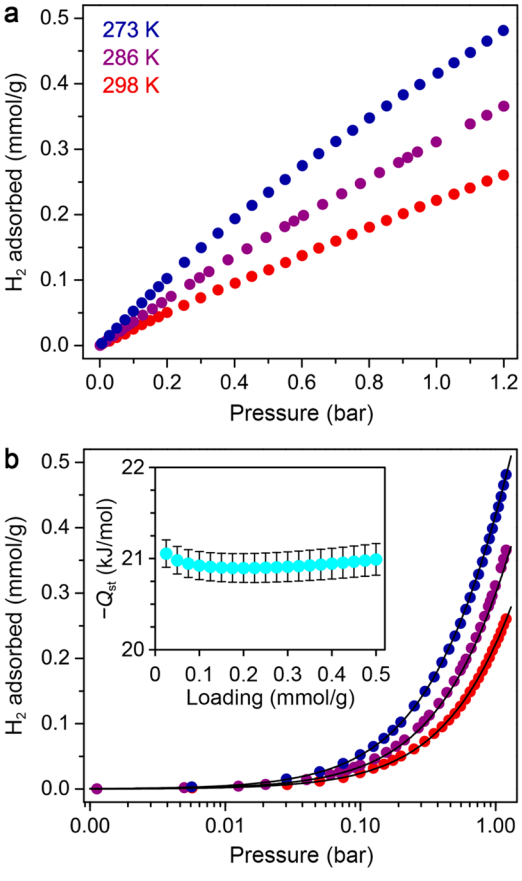

Figure 2. Low-pressure H_2 adsorption isotherms (colored data points) for $V_2Cl_{2.8}$(btdd) at the indicated temperatures with pressure on a linear (a) and logarithmic scale (b). Black lines in part b indicate fits as described in the text. Inset: Isosteric heat of adsorption as a function of H_2 loading.

Infrared Spectroscopy. To confirm vanadium−H_2 bonding in $V_2Cl_{2.8}$(btdd) and further understand the nature of the interaction, we collected *in situ* infrared spectroscopy data upon dosing with H_2 or D_2. Dosing with H_2 at 97 K results in the appearance of two new peaks at 4112 and 3919 cm^{-1} relative to the bare framework spectrum (Figure 3).

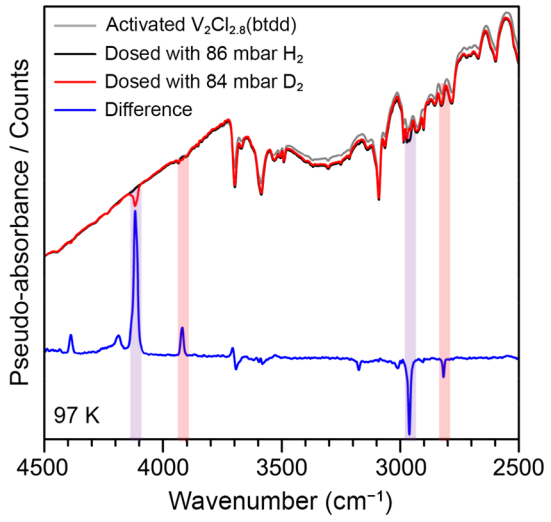

Figure 3. Infrared spectra of activated $V_2Cl_{2.8}$(btdd) (gray) and $V_2Cl_{2.8}$(btdd) dosed with 84 mbar H_2 (red) or 86 mbar D_2 (black). Subtraction of the D_2-dosed spectrum from the H_2-dosed spectrum yields the difference spectrum in blue. Light pink bars highlight bands arising from V−H_2(D_2) interactions and light purple bars indicate physisorptive framework−H_2(D_2) interactions. All spectra were collected at 97 K.

Under analogous conditions, D_2 dosing leads to the appearance of peaks at 2960 and 2800 cm^{-1}, consistent with the band shifts expected for the difference in the reduced mass between H_2 and D_2 under a simple harmonic approximation. As such, we attribute both of these features to stretching modes arising from bound H_2 or D_2. *In situ* infrared spectra collected under varying pressures of H_2 at 120 K revealed that the feature at 3919 cm^{-1} is the first to appear and saturate, and thus is attributed to H_2 strongly bound to the open vanadium(II) sites (Figure S3). The feature at 4112 cm^{-1} is weakly red-shifted relative to the stretching mode of gaseous H_2 (4161 cm^{-1}) and thus is identified as H_2 physisorbed at secondary, nonmetal sites within the material.[47] This assign-

https://doi.org/10.1021/jacs.1c01883
J. Am. Chem. Soc. 2021, 143, 6248−6256

ment is consistent with peaks arising from weak physisorptive interactions in many other framework solids.[38,48]

The vibration of vanadium-bound H_2 is 106 cm^{-1} lower in energy than that observed for nickel(II)-bound H_2 in Ni_2(*m*-dobdc), which occurs at 4025 cm^{-1}.[38] While the degree of the red-shift for the vibration of adsorbed H_2 has been correlated with the magnitude of the adsorption enthalpy, in the case of $V_2Cl_{2.8}$(btdd), the observed bathochromic shift may also reflect backbonding from vanadium into the H_2 σ^* orbital.[47,49] Indeed, population of the H_2 LUMO likely affects the stretch more so than withdrawing electron density from the H_2 HOMO.[38] The relative contributions of backbonding and σ donation are explored more below using electronic structure calculations. Interestingly, while $V_2Cl_{2.8}$(btdd) and Cu-MFU-4*l* exhibit similar metal-bound CO stretches (2081 and 2084 cm^{-1}, respectively), the metal-bound H_2 stretch in Cu-MFU-4*l* occurs at 3252 cm^{-1}, much lower energy than in $V_2Cl_{2.8}$(btdd).[46] Since copper(I) is a d^{10} metal and features high-energy d_π orbitals, the d_π to H_2 LUMO interaction is significant, contributing to a binding enthalpy of −32.3 kJ/mol, which is too exothermic for the targeted storage conditions. These results suggest that H_2 may be a more apt reporter of π-basicity than CO, and they additionally highlight the differing relative contributions from σ donation and backbonding between these two types of metal sites, albeit in different geometries. This observation can help to further inform the type of electronic structure that is competent for achieving H_2 binding with the desired enthalpy range. Overall, the extent of the H_2 redshift trends with the enthalpy of H_2 binding across the three frameworks, increasing from Ni_2(*m*-dobdc) to $V_2Cl_{2.8}$(btdd) to Cu-MFU-4*l*.

The 242 cm^{-1} red shift for H_2 bound in $V_2Cl_{2.8}$(btdd) is much smaller than that typically characterized in molecular dihydrogen complexes (1700−1000 cm^{-1})[50] and is indicative of attenuated dihydrogen activation. Vanadium dihydrogen complexes are rare, and $CpV(CO)_3(H_2)$ is the only example for which an infrared spectrum has been reported.[51,52] Ultraviolet photolysis of this compound in liquid xenon enabled characterization of an H_2 stretch at 2642 cm^{-1}, which is even lower than that observed in the original Kubas complex, although further investigation of this compound was not possible due to its high reactivity. The weaker activation present in $V_2Cl_{2.8}$(btdd) is likely a result of the greater ionic charge at the metal center as well as the weaker surrounding ligand field environment. In summary, these data are consistent with a backbonding mechanism mediated by H_2 donation into the empty vanadium(II) d_{z^2} in $V_2Cl_{2.8}$(btdd).

Variable-temperature infrared spectroscopy provides another well-established method for obtaining thermodynamic parameters of adsorption.[53,49] Accordingly, we collected spectra for $V_2Cl_{2.8}$(btdd) dosed with 18 mbar of H_2 at temperatures ranging from 150 to 185 K (Figure 4). The ensuing absorption peak centered at 3919 cm^{-1} was integrated at each temperature, and a van't Hoff analysis yielded an H_2 binding enthalpy of −21 kJ/mol and entropy of −84 J/(mol·K). While the resulting H_2 adsorption enthalpy is consistent with that determined from gas adsorption data, the entropic term is nearly 20% larger. Interestingly, enthalpy−entropy compensation is well-documented for hydrogen adsorption in zeolites[54] and metal−organic frameworks,[55,56] wherein H_2 is known to bind via σ donation to charge-dense cations. In contrast, $V_2Cl_{2.8}$(btdd) displays a large increase in binding enthalpy relative to Ni_2(*m*-dobdc) without a comparable entropy decrease. As a result, the ΔG of H_2 adsorption at 298 K in $V_2Cl_{2.8}$(btdd) is 4.1 kJ/mol, which is much more favorable than the 11.7 kJ/mol in Ni_2(*m*-dobdc). This result supports a distinct H_2 binding mechanism in $V_2Cl_{2.8}$(btdd) and corroborates the *in situ* IR data, which suggest backbonding in the V^{II}−H_2 interaction. Overall, the data demonstrate that strong orbital-mediated interactions with π-basic metal sites provide a novel means of optimizing the thermodynamics of H_2 adsorption in porous materials for storage applications.

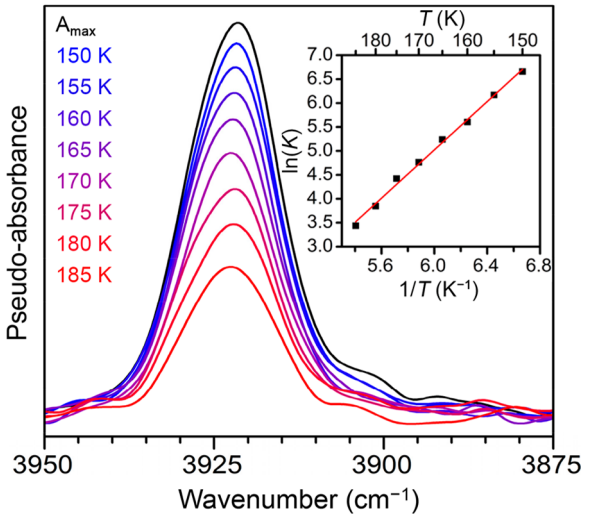

Figure 4. Variable-temperature infrared spectra for $V_2Cl_{2.8}$(btdd) dosed with 18 mbar H_2 (colored lines). A_{max} corresponds to the spectrum collected at 150 K at 1 bar H_2 pressure. The inset shows the van't Hoff plot used to extract enthalpy and entropy values.

Powder Neutron Diffraction. *In situ* powder neutron diffraction data were collected upon dosing with D_2 to obtain the first structural characterization of a vanadium(II)−dihydrogen complex (see details in the Supporting Information). Data were first collected for an activated sample of $V_2Cl_{2.8}$(btdd) at 100 K. The sample was then heated to 200 K, dosed with approximately 0.75 equiv of D_2 per V^{II} site, and allowed to equilibrate before being cooled again to 100 K for data collection. Given the exceptionally small neutron scattering cross section of vanadium, we also collected powder X-ray diffraction data at 100 K for a sample of $V_2Cl_{2.8}$(btdd) dosed with 0.75 equiv of D_2 to obtain refined vanadium positions and thermal parameters. These values were then applied to refine the structure against the neutron diffraction data (Figures S4 − S7).

Rietveld refinement of the activated and D_2-dosed structures revealed that the V−Cl equatorial bonds contract and the Cl−V−Cl bond angle decreases slightly upon D_2 binding (from 175.8(6)° to 167.9(7)°; Figure 1b,c). These changes lead to a slight shift of the vanadium center out of the equatorial ligand plane, presumably to enhance metal orbital overlap with D_2. In particular, the observed Cl−V−Cl bend is consistent with a lowering of the d_{z^2}-based σ^* orbital, which results in a closer energy match with the H_2 HOMO. Indeed, a similar structural change is observed upon N_2 binding in $V_2Cl_{2.8}$(btdd).[44] The resulting V−D_2(centroid) distance of 1.966(8) Å is the shortest yet reported for a MOF. While we were unable to resolve the D−D bond, the short metal−D_2 distance is consistent with a Kubas-type interaction.

High-Pressure H_2 Adsorption. The high H_2 uptake in $V_2Cl_{2.8}$(btdd) at low pressures motivated us to examine

https://doi.org/10.1021/jacs.1c01883
J. Am. Chem. Soc. 2021, 143, 6248−6256

ambient temperature uptake at high pressures near target conditions for on-board storage (Figures 5 and S9). Here, total

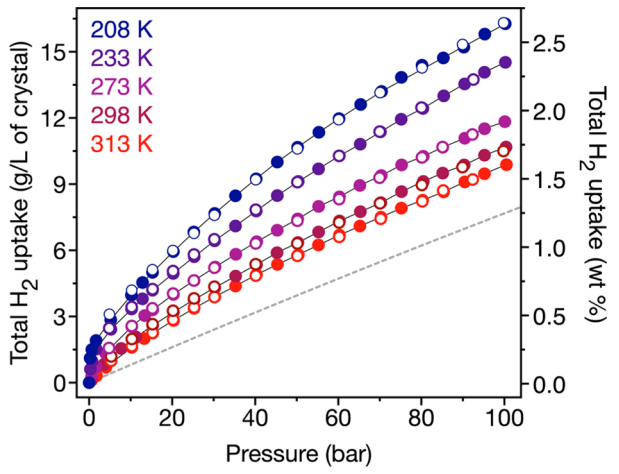

Figure 5. High-pressure H_2 isotherms obtained for $V_2Cl_{2.8}$(btdd) at near ambient temperatures. Filled and open circles represent adsorption and desorption, respectively. Solid lines indicate fits with a dual-site Langmuir–Freundlich model. The gray dashed line represents the volumetric density of compressed hydrogen at 298 K.

uptake was determined from the raw data (i.e., excess uptake) by taking into account bulk hydrogen density and the pore volume of the material (see the Supporting Information). At 298 K and 100 bar, the total volumetric hydrogen uptake in $V_2Cl_{2.8}$(btdd) (based on crystallographic density) is 10.7 g/L. This uptake represents a 38% increase over compressed hydrogen under the same conditions and a 27% enhancement over that of the best performing physisorptive material.[18] The latter comparison highlights the importance of optimizing adsorption enthalpy when considering storage performance at ambient temperatures. Despite this, owing to its larger pore size (1.12 cm^3/g versus 0.56 cm^3/g) and a lower volumetric density of primary binding sites, the total volumetric uptake in $V_2Cl_{2.8}$(btdd) is lower than that in Ni_2(*m*-dobdc) at 298 K and 100 bar (11.9 g/L). However, under these conditions, the total *gravimetric* H_2 uptake in $V_2Cl_{2.8}$(btdd) is 1.64 wt %, which is 60% greater than that in Ni_2(*m*-dobdc). In fact, the room temperature total gravimetric uptake of $V_2Cl_{2.8}$(btdd) is comparable to that of Ni_2(*m*-dobdc) at 233 K. At 208 K and 50 bar, $V_2Cl_{2.8}$(btdd) achieves a capacity of 10.7 g/L, and at 208 K and 150 bar, the material capacity nearly doubles to 20 g/L.

A closer examination of the excess adsorption isotherms aids in an understanding of the influence of the exposed vanadium(II) sites on H_2 uptake (see the Supporting Information and Figure S10). Here, we assume that all uptake below 2.5 mmol/g (corresponding to saturation of the V^{II} sites) is due to vanadium–H_2 complexation, although some small amount of physisorption under these conditions cannot be excluded. At 298 K and 5 bar, the H_2 excess uptake corresponds to less than 25% primary site surface coverage, while at 40 bar of H_2, the uptake corresponds to one H_2 per vanadium(II) center. Saturation at 40 bar is consistent with a model isotherm generated from the experimentally obtained enthalpy and entropy parameters, which shows 90% vanadium surface coverage at 50 bar (Figure S11). In contrast, less than 33% of the nickel(II) sites are occupied in Ni_2(*m*-dobdc) at 298 K and a higher pressure of 100 bar.

Significantly, for operation at 298 K between 5 and 100 bar, the usable volumetric capacity of $V_2Cl_{2.8}$(btdd) is 30% more than that achievable with compressed H_2 under the same conditions (Figures 6). Further improvements are achieved by

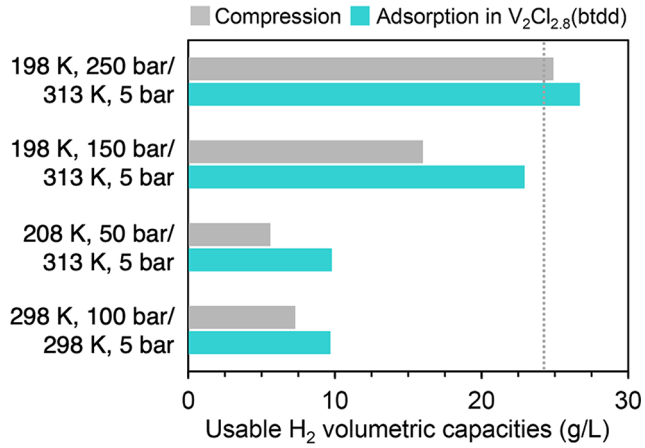

Figure 6. A comparison of usable volumetric H_2 capacities using $V_2Cl_{2.8}$(btdd) and compression under four different loading/discharging conditions. The dotted gray line indicates usable volumetric capacity for 350 bar compressed storage at 298 K.

optimizing the vanadium(II) surface coverage (Figure S12), for example, narrowing the pressure range from 5 to 50 bar and including a temperature swing from 208 to 313 K. These conditions give rise to a usable capacity of 9.8 g/L, a significant 75% improvement over compressed hydrogen under the same conditions. Thus, in addition to its excellent performance at higher pressures, $V_2Cl_{2.8}$(btdd) may be of interest for low-pressure H_2 storage applications. For greater energy density requirements, a larger pressure and temperature swing can generate usable capacities greater than those achieved with 350 bar compressed storage (23 g/L). For example, loading at 198 K and 250 bar and discharging at 313 K and 5 bar provide 26 g/L of useable hydrogen.

Electronic Structure Calculations. Density functional theory was employed to better understand the orbital interactions involved in dihydrogen complexation in $V_2Cl_{2.8}$(btdd). A two-vanadium cluster model was chosen as a representation of the structure (Figure 7). The overall neutral cluster contains one square pyramidal vanadium(II) center, one coordinatively saturated vanadium(III) center, three triazoles, one triazolate, and four chlorides. In general, the

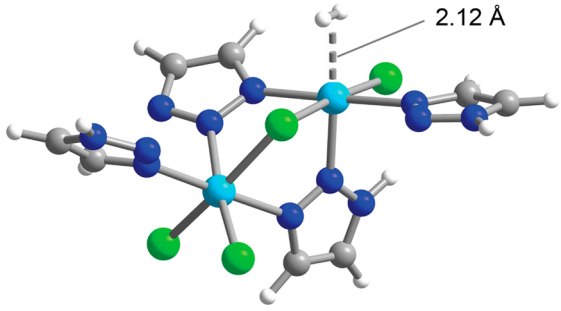

Figure 7. Structure of the two-vanadium cluster model used to study the V^{II}–H_2 interaction in $V_2Cl_{2.8}$(btdd) and for energy decomposition analysis.

https://doi.org/10.1021/jacs.1c01883
J. Am. Chem. Soc. 2021, 143, 6248–6256

cluster triazoles and triazolate are likely more electron rich than those in the actual framework, wherein each triazolate is bound to three positively charged vanadium centers. A CRENBL basis with a fit-CRENBL effective core potential,[56] augmented with *f*-polarization at the metal site,[57] was used for geometry optimizations. The experimental structure from neutron diffraction was used to generate an initial model structure, and all nuclear degrees of freedom in the cluster model were allowed to relax using the ωB97M-v functional.[58,59] The optimized structure exhibits a $V^{II}-H_2$ distance of 2.11 Å with dihydrogen aligned along the Cl−V−Cl direction. The calculated redshift in the H−H stretch for this structure is 240 cm^{-1}, consistent with the experimental value of 193 cm^{-1}.

An energy decomposition analysis (EDA) was performed using absolutely localized molecular orbitals.[60,61] In this analysis, the interaction between the two fragments, i.e., the vanadium(II) center and the H_2 molecule, is partitioned into three contributions, namely, frozen, polarization, and charge transfer terms. Briefly, the frozen term contains three interactions that arise without relaxation of the fragment orbitals: permanent electrostatics, Pauli repulsion, and dispersion interactions. The polarization term is the favorable interaction between the two self-contained fragments. Lastly, the charge transfer term accounts for the energy lowering that occurs from orbital mixing between the two fragments. This latter term maps directly to the general concept of orbital interactions. In the optimized cluster model, the large charge transfer component facilitates a strong interaction resulting in a short metal−H_2 distance, which increases the repulsive frozen interactions (Table 1). Indeed, the frozen interaction

Table 1. Results of Energy Decomposition Analysis of the $V^{II}-H_2$ Interaction in the Fully Relaxed $V_2Cl_{2.8}$(btdd) Cluster Model

Component	Energy (kJ/mol)
Frozen	7.57
Polarization	−6.08
Charge transfer	−31.92
Total	−30.96
Charge transfer components	Energy (kJ/mol)
H_2 σ (HOMO) → V d_z2	−19.34
V d_π → H_2 σ^* (LUMO)	−12.58

contribution is greater in magnitude than the polarization term, in contrast to what has been calculated for binding at Lewis acidic sites, such as in Co_2(*m*-dobdc).[38] Overall, this orbital-mediated interaction results in a binding energy of −30.1 kJ/mol and a calculated enthalpy of −19.9 kJ/mol (Table S4). The relative contributions of the frozen, polarization, and charge transfer terms were consistent across different functionals (Figure S13).

The charge transfer component can be further divided into forward and backdonation, or ligand−to−metal and metal−to−ligand contributions. In this case, the interaction between the H_2 σ orbital and vanadium d_{z^2} orbital is the primary forward contribution, and the interaction between the vanadium d_π and H_2 σ^* orbital is the dominant backbonding contribution (Table 1 and Figure S14). In the fully relaxed cluster model, the ligand−to−metal interaction is the major contributor to charge transfer, accounting for 60% of the stabilization. This highlights the importance of an empty d_{z^2} orbital and partly rationalizes why similarly strong binding is not observed in other azolate-based frameworks with exposed chromium(II) sites, which have a partially occupied d_{z^2} orbital.[62]

Lastly, to better capture the electronic structure of the framework vanadium(II) centers, we also performed an EDA with two additional cluster models: one with the nuclear coordinates frozen to correspond with the experimental structure wherein the hydrogen was allowed to relax, and one in which the vanadium center and hydrogen were both allowed to relax (Table S5). For both calculations, the relative contributions were similar to the fully relaxed model, and the resulting final binding energies were −27.6 and −27.2 kJ/mol, respectively.

CONCLUSION

The pursuit of adsorbents capable of ambient-temperature hydrogen storage has largely focused on those featuring coordinatively unsaturated metal sites that can polarize and bind H_2. Inspired by strong orbital-mediated metal−H_2 interactions in molecular complexes, we have targeted an alternative strategy to engender slightly stronger metal−dihydrogen binding in MOFs, using weakly π-basic metal sites capable of backbonding interactions with H_2. We validated this approach using the framework $V_2Cl_{2.8}$(btdd), which contains a high-density of vanadium(II) sites capable of backbonding interactions with H_2. We have characterized this type of interaction for the first time using powder neutron and X-ray diffraction data, as well as variable-temperature infrared spectroscopy. Significantly, the weak Kubas-type interaction exemplified here results in a binding enthalpy of −21 kJ/mol, within the optimal range for ambient hydrogen storage applications, and gives rise to volumetric capacities that are greater than those achieved with compressed H_2 under a range of operating conditions. Future efforts will be directed toward synthesizing frameworks with a higher density of vanadium(II) sites which may be a viable approach to achieve densities greater than that achievable with compressed H_2 at 700 bar. For example, the hypothetical materials V_2Cl_2(btdd) and V_2Cl_2(bbta) (H_2bbta= 1*H*,5*H*-benzo(1,2-d:4,5-*d*′)-bistriazole)[63] would exhibit 1.7 and 2.3 times greater metal site densities, respectively. Importantly, frameworks with π-basic binding sites, such as $V_2Cl_{2.8}$(btdd), expand the type of metal−adsorbate interactions that can be interrogated beyond what has been possible with exposed Lewis acid sites.

ASSOCIATED CONTENT

Supporting Information

The Supporting Information is available free of charge at https://pubs.acs.org/doi/10.1021/jacs.1c01883.

Experimental details (PDF)

Accession Codes

CCDC 2063531−2063532 contain the supplementary crystallographic data for this paper. These data can be obtained free of charge via www.ccdc.cam.ac.uk/data_request/cif, or by emailing data_request@ccdc.cam.ac.uk, or by contacting The Cambridge Crystallographic Data Centre, 12 Union Road, Cambridge CB2 1EZ, UK; fax: +44 1223 336033.

https://doi.org/10.1021/jacs.1c01883
J. Am. Chem. Soc. 2021, 143, 6248−6256

AUTHOR INFORMATION

Corresponding Author

Jeffrey R. Long − *Department of Chemistry, University of California, Berkeley, California 94720, United States; Materials Sciences Division, Lawrence Berkeley National Laboratory, Berkeley, California 94720, United States; Department of Chemical and Biomolecular Engineering, University of California, Berkeley, California 94720, United States;* orcid.org/0000-0002-5324-1321; Email: jrlong@berkeley.edu

Authors

David E. Jaramillo − *Department of Chemistry, University of California, Berkeley, California 94720, United States; Materials Sciences Division, Lawrence Berkeley National Laboratory, Berkeley, California 94720, United States;* orcid.org/0000-0002-3068-4963

Henry Z. H. Jiang − *Department of Chemistry, University of California, Berkeley, California 94720, United States; Materials Sciences Division, Lawrence Berkeley National Laboratory, Berkeley, California 94720, United States*

Hayden A. Evans − *Center for Neutron Research, National Institute of Standards and Technology, Gaithersburg, Maryland 20899, United States;* orcid.org/0000-0002-1331-4274

Romit Chakraborty − *Department of Chemistry, University of California, Berkeley, California 94720, United States; Chemical Sciences Division, Lawrence Berkeley National Laboratory, Berkeley, California 94720, United States*

Hiroyasu Furukawa − *Department of Chemistry, University of California, Berkeley, California 94720, United States; Materials Sciences Division, Lawrence Berkeley National Laboratory, Berkeley, California 94720, United States;* orcid.org/0000-0002-6082-1738

Craig M. Brown − *Center for Neutron Research, National Institute of Standards and Technology, Gaithersburg, Maryland 20899, United States; Department of Chemical and Biomolecular Engineering, University of Delaware, Newark, Delaware 19716, United States*

Martin Head-Gordon − *Department of Chemistry, University of California, Berkeley, California 94720, United States; Chemical Sciences Division, Lawrence Berkeley National Laboratory, Berkeley, California 94720, United States;* orcid.org/0000-0002-4309-6669

Complete contact information is available at: https://pubs.acs.org/10.1021/jacs.1c01883

Notes

The authors declare the following competing financial interest(s): D.E.J. has financial interest in Verne, Inc., which is developing hydrogen storage technologies. The University of California, Berkeley has filed a patent application on the work reported herein, on which J.R.L. and D.E.J are listed as inventors.

ACKNOWLEDGMENTS

The authors gratefully acknowledge support from the Hydrogen Materials—Advanced Research Consortium (HyMARC), established as part of the Energy Materials Network under the U.S. Department of Energy (DOE), Office of Energy Efficiency and Renewable Energy (EERE), Hydrogen and Fuel Cell Technologies Office, under Contract Number DE-AC02-05CH11231 with Lawrence Berkeley National Laboratory (LBNL). Powder X-ray diffraction data were collected on beamline 17-BM at the Advanced Photon Source at Argonne National Laboratory, which is supported by the U.S. Department of Energy, Office of Science, Office of Basic Energy Sciences under Contract No. DEAC02-06CH11357. We thank the National Science Foundation for graduate research fellowship support of D.E.J., Benjamin Trump and Douglas A. Reed for helpful discussions, and Dr. Katie R. Meihaus for editorial assistance.

REFERENCES

(1) Nocera, D. G. Chemistry of Personalized Solar Energy. *Inorg. Chem.* **2009**, *48*, 10001−10017.

(2) Rosenzweig, C.; Karoly, D.; Vicarelli, M.; Neofotis, P.; Wu, Q.; Casassa, G.; Menzel, A.; Root, T. L.; Estrella, N.; Seguin, B.; Tryjanowski, P.; Liu, C.; Rawlins, S.; Imeson, A. Attributing Physical and Biological Impacts to Anthropogenic Climate Change. *Nature* **2008**, *453*, 353−357.

(3) U.S. Energy Information Administration. Total Energy Annual Data - U.S. Energy Information Administration (EIA) https://www.eia.gov/totalenergy/data/annual/index.php (accessed Oct 9, 2020).

(4) Davis, S. J.; Lewis, N. S.; Shaner, M.; Aggarwal, S.; Arent, D.; Azevedo, I. L.; Benson, S. M.; Bradley, T.; Brouwer, J.; Chiang, Y. M.; Clack, C. T. M.; Cohen, A.; Doig, S.; Edmonds, J.; Fennell, P.; Field, C. B.; Hannegan, B.; Hodge, B. M.; Hoffert, M. I.; Ingersoll, E.; Jaramillo, P.; Lackner, K. S.; Mach, K. J.; Mastrandrea, M.; Ogden, J.; Peterson, P. F.; Sanchez, D. L.; Sperling, D.; Stagner, J.; Trancik, J. E.; Yang, C. J.; Caldeira, K. Net-Zero Emissions Energy Systems. *Science* **2018**, *360*, eaas9793.

(5) van Renssen, S. The Hydrogen Solution? *Nat. Clim. Change* **2020**, *10*, 799−801.

(6) DeLuchi, M. A. Hydrogen Vehicles: An Evaluation of Fuel Storage, Performance, Safety, Environmental Impacts, and Cost. *Int. J. Hydrogen Energy* **1989**, *14*, 81−130.

(7) Tollefson, J. Hydrogen Vehicles: Fuel of the Future? *Nature* **2010**, *464*, 1262−1264.

(8) Hua, T.; Ahluwalia, R.; Eudy, L.; Singer, G.; Jermer, B.; Asselin-Miller, N.; Wessel, S.; Patterson, T.; Marcinkoski, J. Status of Hydrogen Fuel Cell Electric Buses Worldwide. *J. Power Sources* **2014**, *269*, 975−993.

(9) Mason, J. A.; Veenstra, M.; Long, J. R. Evaluating Metal-Organic Frameworks for Natural Gas Storage. *Chem. Sci.* **2014**, *5*, 32−51.

(10) Eberle, U.; Felderhoff, M.; Schüth, F. Chemical and Physical Solutions for Hydrogen Storage. *Angew. Chem., Int. Ed.* **2009**, *48*, 6608−6630.

(11) Kurtz, J.; Sprik, S.; Bradley, T. H. Review of Transportation Hydrogen Infrastructure Performance and Reliability. *Int. J. Hydrogen Energy* **2019**, *44*, 12010−12023.

(12) Hosseini, M.; Dincer, I.; Naterer, G. F.; Rosen, M. A. Thermodynamic Analysis of Filling Compressed Gaseous Hydrogen Storage Tanks. *Int. J. Hydrogen Energy* **2012**, *37*, 5063−5071.

(13) Yoshida, T.; Kojima, K. Toyota MIRAI Fuel Cell Vehicle and Progress toward a Future Hydrogen Society. *Electrochem. Soc. Interface* **2015**, *24*, 45−49.

(14) Chahine, R.; Bose, T. K. Low-Pressure Adsorption Storage of Hydrogen. *Int. J. Hydrogen Energy* **1994**, *19*, 161−164.

(15) Kaye, S. S.; Dailly, A.; Yaghi, O. M.; Long, J. R. Impact of Preparation and Handling on the Hydrogen Storage Properties of Zn_4O(1,4-benzenedicarboxylate)$_3$ (MOF-5). *J. Am. Chem. Soc.* **2007**, *129*, 14176−14177.

(16) Wong-Foy, A. G.; Matzger, A. J.; Yaghi, O. M. Exceptional H_2 Saturation Uptake in Microporous Metal-Organic Frameworks. *J. Am. Chem. Soc.* **2006**, *128*, 3494−3495.

(17) Ahmed, A.; Seth, S.; Purewal, J.; Wong-Foy, A. G.; Veenstra, M.; Matzger, A. J.; Siegel, D. J. Exceptional Hydrogen Storage Achieved by Screening Nearly Half a Million Metal-Organic Frameworks. *Nat. Commun.* **2019**, *10*, 1−9.

(18) Chen, Z.; Li, P.; Anderson, R.; Wang, X.; Zhang, X.; Robison, L.; Redfern, L. R.; Moribe, S.; Islamoglu, T.; Gómez-Gualdrón, D. A.; Yildirim, T.; Stoddart, J. F.; Farha, O. K. Balancing Volumetric and Gravimetric Uptake in Highly Porous Materials for Clean Energy. *Science* **2020**, *368*, 297−303.
(19) Purewal, J.; Veenstra, M.; Tamburello, D.; Ahmed, A.; Matzger, A. J.; Wong-Foy, A. G.; Seth, S.; Liu, Y.; Siegel, D. J. Estimation of System-Level Hydrogen Storage for Metal-Organic Frameworks with High Volumetric Storage Density. *Int. J. Hydrogen Energy* **2019**, *44*, 15135−15145.
(20) Petitpas, G.; Bénard, P.; Klebanoff, L. E.; Xiao, J.; Aceves, S. A Comparative Analysis of the Cryo-Compression and Cryo-Adsorption Hydrogen Storage Methods. *Int. J. Hydrogen Energy* **2014**, *39*, 10564−10584.
(21) Hardy, B.; Tamburello, D.; Corgnale, C. Hydrogen Storage Adsorbent Systems Acceptability Envelope. *Int. J. Hydrogen Energy* **2018**, *43*, 19528−19539.
(22) Barthelemy, H.; Weber, M.; Barbier, F. Hydrogen Storage: Recent Improvements and Industrial Perspectives. *Int. J. Hydrogen Energy* **2017**, *42*, 7254−7262.
(23) Allendorf, M. D.; Hulvey, Z.; Gennett, T.; Ahmed, A.; Autrey, T.; Camp, J.; Seon Cho, E.; Furukawa, H.; Haranczyk, M.; Head-Gordon, M.; Jeong, S.; Karkamkar, A.; Liu, D. J.; Long, J. R.; Meihaus, K. R.; Nayyar, I. H.; Nazarov, R.; Siegel, D. J.; Stavila, V.; Urban, J. J.; Veccham, S. P.; Wood, B. C. An Assessment of Strategies for the Development of Solid-State Adsorbents for Vehicular Hydrogen Storage. *Energy Environ. Sci.* **2018**, *11*, 2784−2812.
(24) Sharaf, O. Z.; Orhan, M. F. An Overview of Fuel Cell Technology: Fundamentals and Applications. *Renewable Sustainable Energy Rev.* **2014**, *32*, 810−853.
(25) Bhatia, S. K.; Myers, A. L. Optimum Conditions for Adsorptive Storage. *Langmuir* **2006**, *22*, 1688−1700.
(26) Bae, Y. S.; Snurr, R. Q. Optimal Isosteric Heat of Adsorption for Hydrogen Storage and Delivery Using Metal-Organic Frameworks. *Microporous Mesoporous Mater.* **2010**, *132*, 300−303.
(27) He, T.; Pachfule, P.; Wu, H.; Xu, Q.; Chen, P. Hydrogen Carriers. *Nat. Rev. Mater.* **2016**, *1*, 16059.
(28) Li, J. R.; Kuppler, R. J.; Zhou, H. C. Selective Gas Adsorption and Separation in Metal-Organic Frameworks. *Chem. Soc. Rev.* **2009**, *38*, 1477−1504.
(29) Gardner, G. B.; Venkataraman, D.; Moore, J. S.; Lee, S. Spontaneous Assembly of a Hinged Coordination Network. *Nature* **1995**, *374*, 792−795.
(30) Yaghi, O. M.; Li, G.; Li, H. Selective Binding and Removal of Guests in a Microporous Metal−Organic Framework. *Nature* **1995**, *378*, 703−706.
(31) Furukawa, H.; Cordova, K. E.; O'Keeffe, M.; Yaghi, O. M. The Chemistry and Applications of Metal-Organic Frameworks. *Science* **2013**, *341*, 1230444.
(32) Langmi, H. W.; Ren, J.; North, B.; Mathe, M.; Bessarabov, D. Hydrogen Storage in Metal-Organic Frameworks: A Review. *Electrochim. Acta* **2014**, *128*, 368−392.
(33) Schoedel, A.; Ji, Z.; Yaghi, O. M. The Role of Metal−Organic Frameworks in a Carbon-Neutral Energy Cycle. *Nat. Energy* **2016**, *16034*, 1−13.
(34) Krawiec, P.; Kramer, M.; Sabo, M.; Kunschke, R.; Fröde, H.; Kaskel, S. Improved Hydrogen Storage in the Metal-Organic Framework $Cu_3(BTC)_2$. *Adv. Eng. Mater.* **2006**, *8*, 293−296.
(35) Dinča, M.; Dailly, A.; Liu, Y.; Brown, C. M.; Neumann, D. A.; Long, J. R. Hydrogen Storage in a Microporous Metal-Organic Framework with Exposed Mn^{2+} Coordination Sites. *J. Am. Chem. Soc.* **2006**, *128*, 16876−16883.
(36) Lee, K.; Howe, J. D.; Lin, L. C.; Smit, B.; Neaton, J. B. Small-Molecule Adsorption in Open-Site Metal-Organic Frameworks: A Systematic Density Functional Theory Study for Rational Design. *Chem. Mater.* **2015**, *27*, 668−678.
(37) Bloch, E. D.; Hudson, M. R.; Mason, J. A.; Chavan, S.; Crocellà, V.; Howe, J. D.; Lee, K.; Dzubak, A. L.; Queen, W. L.; Zadrozny, J. M.; Geier, S. J.; Lin, L. C.; Gagliardi, L.; Smit, B.; Neaton, J. B.; Bordiga, S.; Brown, C. M.; Long, J. R. Reversible CO Binding Enables Tunable CO/H_2 and CO/N_2 Separations in Metal-Organic Frameworks with Exposed Divalent Metal Cations. *J. Am. Chem. Soc.* **2014**, *136*, 10752−10761.
(38) Kapelewski, M. T.; Geier, S. J.; Hudson, M. R.; Stück, D.; Mason, J. A.; Nelson, J. N.; Xiao, D. J.; Hulvey, Z.; Gilmour, E.; Fitzgerald, S. A.; Head-Gordon, M.; Brown, C. M.; Long, J. R. M_2(*m*-dobdc) (M = Mg, Mn, Fe, Co, Ni) Metal-Organic Frameworks Exhibiting Increased Charge Density and Enhanced H_2 Binding at the Open Metal Sites. *J. Am. Chem. Soc.* **2014**, *136*, 12119−12129.
(39) Kapelewski, M. T.; Runčevski, T.; Tarver, J. D.; Jiang, H. Z. H.; Hurst, K. E.; Parilla, P. A.; Ayala, A.; Gennett, T.; Fitzgerald, S. A.; Brown, C. M.; Long, J. R. Record High Hydrogen Storage Capacity in the Metal-Organic Framework Ni2(m-Dobdc) at Near-Ambient Temperatures. *Chem. Mater.* **2018**, *30*, 8179−8189.
(40) Kubas, G. J.; Ryan, R. R.; Swanson, B. I.; Vergamini, P. J.; Wasserman, H. J. Characterization of the First Examples of Isolable Molecular Hydrogen Complexes, $M(CO)_3(PR_3)_2(H_2)$ (M = Mo, W; R = Cy, i-Pr). Evidence for a Side-on Bonded H2Ligand. *J. Am. Chem. Soc.* **1984**, *106*, 451−452.
(41) Kubas, G. J. Chemistry of Saturated Molecules. *Proc. Natl. Acad. Sci. U. S. A.* **2007**, *104*, 6901−6907.
(42) Crabtree, R. H. Dihydrogen Complexation. *Chem. Rev.* **2016**, *116*, 8750−8769.
(43) Kubas, G. J. Fundamentals of H_2 Binding and Reactivity on Transition Metals Underlying Hydrogenase Function and H_2 Production and Storage. *Chem. Rev.* **2007**, *107*, 4152−4205.
(44) Jaramillo, D. E.; Reed, D. A.; Jiang, H. Z. H.; Oktawiec, J.; Mara, M. W.; Forse, A. C.; Lussier, D. J.; Murphy, R. A.; Cunningham, M.; Colombo, V.; Shuh, D. K.; Reimer, J. A.; Long, J. R. Selective Nitrogen Adsorption via Backbonding in a Metal−Organic Framework with Exposed Vanadium Sites. *Nat. Mater.* **2020**, *19*, 517−521.
(45) Lee, K.; Isley, W. C.; Dzubak, A. L.; Verma, P.; Stoneburner, S. J.; Lin, L. C.; Howe, J. D.; Bloch, E. D.; Reed, D. A.; Hudson, M. R.; Brown, C. M.; Long, J. R.; Neaton, J. B.; Smit, B.; Cramer, C. J.; Truhlar, D. G.; Gagliardi, L. Design of a Metal-Organic Framework with Enhanced Back Bonding for Separation of N_2 and CH_4. *J. Am. Chem. Soc.* **2014**, *136*, 698−704.
(46) Denysenko, D.; Grzywa, M.; Jelic, J.; Reuter, K.; Volkmer, D. Scorpionate-Type Coordination in MFU-4l Metal-Organic Frameworks: Small-Molecule Binding and Activation upon the Thermally Activated Formation of Open Metal Sites. *Angew. Chem., Int. Ed.* **2014**, *53*, 5832−5836.
(47) Fitzgerald, S. A.; Burkholder, B.; Friedman, M.; Hopkins, J. B.; Pierce, C. J.; Schloss, J. M.; Thompson, B.; Rowsell, J. L. C. Metal-Specific Interactions of H_2 Adsorbed within Isostructural Metal-Organic Frameworks. *J. Am. Chem. Soc.* **2011**, *133*, 20310−20318.
(48) Vitillo, J. G.; Regli, L.; Chavan, S.; Ricchiardi, G.; Spoto, G.; Dietzel, P. D. C.; Bordiga, S.; Zecchina, A. Role of Exposed Metal Sites in Hydrogen Storage in MOFs. *J. Am. Chem. Soc.* **2008**, *130*, 8386−8396.
(49) Areán, C. O.; Chavan, S.; Cabello, C. P.; Garrone, E.; Palomino, G. T. Thermodynamics of Hydrogen Adsorption on Metal-Organic Frameworks. *ChemPhysChem* **2010**, *11*, 3237−3242.
(50) Kubas, G. J. Molecular Hydrogen Complexes: Coordination of a σ Bond to Transition Metals. *Acc. Chem. Res.* **1988**, *21*, 120−128.
(51) Haward, M.; Goerge, M.; S, H.; Poliakoff, M. Non-Classical Dihydrogen Complexes of Vanadium : The Spectroscopic Characterization of $[(C_5H_5)V(CO)_3(H_2)]$ in Solution at Both Cryogenic and Room Temperatures. *J. Chem. Soc., Chem. Commun.* **1990**, 913−915.
(52) Haward, M. T.; George, M. W.; Hamley, P.; Poliakoff, M. Dihydride versus Dihydrogen Complex; the Photochemical Reaction of $[(H_5\text{-}C_5H_5)M(CO)_4]$ (M = V, Nb and Ta) with Hydrogen in Solution at Both Cryogenic and Room Temperatures. *J. Chem. Soc., Chem. Commun.* **1991**, *0*, 1101−1103.
(53) Garrone, E.; Areán, C. O. Variable Temperature Infrared Spectroscopy: A Convenient Tool for Studying the Thermodynamics of Weak Solid−Gas Interactions. *Chem. Soc. Rev.* **2005**, *34*, 846−857.

https://doi.org/10.1021/jacs.1c01883
J. Am. Chem. Soc. 2021, 143, 6248−6256

(54) Garrone, E.; Bonelli, B.; Otero Areán, C. Enthalpy-Entropy Correlation for Hydrogen Adsorption on Zeolites. *Chem. Phys. Lett.* **2008**, *456*, 68−70.
(55) Areán, C. O.; Chavan, S.; Cabello, C. P.; Garrone, E.; Palomino, G. T. Thermodynamics of Hydrogen Adsorption on Metal-Organic Frameworks. *ChemPhysChem* **2010**, *11*, 3237−3242.
(56) Pacios, L. F.; Christiansen, P. A. Ab Initio Relativistic Effective Potentials with Spin-Orbit Operators. I. Li through Ar. *J. Chem. Phys.* **1985**, *82*, 2664−2671.
(57) Liang, W. Z.; Bell, A. T.; Head-Gordon, M.; Chakraborty, A. K. Density Functional Theory Investigations of the Direct Oxidation of Methane on an Fe-Exchanged Zeolite. *J. Phys. Chem. B* **2004**, *108*, 4362−4368.
(58) Mardirossian, N.; Head-Gordon, M. ωB97M-V: A Combinatorially Optimized, Range-Separated Hybrid, Meta-GGA Density Functional with VV10 Nonlocal Correlation. *J. Chem. Phys.* **2016**, *144*, 214110.
(59) Mardirossian, N.; Head-Gordon, M. Thirty Years of Density Functional Theory in Computational Chemistry: An Overview and Extensive Assessment of 200 Density Functionals. *Mol. Phys.* **2017**, *115*, 2315−2372.
(60) Khaliullin, R. Z.; Cobar, E. A.; Lochan, R. C.; Bell, A. T.; Head-Gordon, M. Unravelling the Origin of Intermolecular Interactions Using Absolutely Localized Molecular Orbitals. *J. Phys. Chem. A* **2007**, *111*, 8753−8765.
(61) Horn, P. R.; Mao, Y.; Head-Gordon, M. Probing Non-Covalent Interactions with a Second Generation Energy Decomposition Analysis Using Absolutely Localized Molecular Orbitals. *Phys. Chem. Chem. Phys.* **2016**, *18*, 23067−23079.
(62) Bloch, E. D.; Queen, W. L.; Hudson, M. R.; Mason, J. A.; Xiao, D. J.; Murray, L. J.; Flacau, R.; Brown, C. M.; Long, J. R. Hydrogen Storage and Selective, Reversible O_2 Adsorption in a Metal−Organic Framework with Open Chromium(II) Sites. *Angew. Chem., Int. Ed.* **2016**, *55*, 8605−8609.
(63) Liao, P. Q.; Li, X. Y.; Bai, J.; He, C. T.; Zhou, D. D.; Zhang, W. X.; Zhang, J. P.; Chen, X. M. Drastic Enhancement of Catalytic Activity via Post-Oxidation of a Porous MnII Triazolate Framework. *Chem. - Eur. J.* **2014**, *20*, 11303−11307.

https://doi.org/10.1021/jacs.1c01883
J. Am. Chem. Soc. 2021, 143, 6248−6256